


## Article

# Element Strategy Using Ru-Mn Substitution in CuO-CaCu<sub>3</sub>Ru<sub>4</sub>O<sub>12</sub> Composite Ceramics with High Electrical Conductivity

Akihiro Tsuruta <sup>1,\*</sup>, Masashi Mikami <sup>1</sup>, Yoshiaki Kinemuchi <sup>1</sup>, Ichiro Terasaki <sup>1,2</sup> , Norimitsu Murayama <sup>3</sup> and Woosuck Shin <sup>1</sup>

<sup>1</sup> National Institute of Advanced Industrial Science and Technology (AIST), Shimo-Shidami, Moriyama-ku, Nagoya 463-8560, Japan; m-mikami@aist.go.jp (M.M.); y.kinemuchi@aist.go.jp (Y.K.); terra@cc.nagoya-u.ac.jp (I.T.); w.shin@aist.go.jp (W.S.)

<sup>2</sup> Department of Physics, Nagoya University, Furo-cho, Chikusa-ku, Nagoya 464-8602, Japan

<sup>3</sup> National Institute of Advanced Industrial Science and Technology (AIST), 1-1-1 Higashi, Tsukuba 305-8565, Japan; n-murayama@aist.go.jp

\* Correspondence: a.tsuruta@aist.go.jp; Tel.: +81-52-736-7481

Academic Editor: Stevin Snellius Pramana

Received: 15 May 2017; Accepted: 8 July 2017; Published: 10 July 2017

**Abstract:** CaCu<sub>3</sub>Ru<sub>4-x</sub>Mn<sub>x</sub>O<sub>12</sub> bulks with various substitution amounts  $x$  and sintering additive CuO (20 vol.%) were prepared, and the influence of  $x$  on the electrical conductivity in a wide temperature range (8–900 K) was investigated. Microstructural observations showed an enhancement of bulk densification upon Mn substitution. Although the resistivity increased with increasing  $x$ , the resistivity was as low as a few mΩcm even in the sample with  $x = 2.00$ , where half of Ru is substituted by Mn. This high conductivity despite the loss of Ru 4d conduction following the substitution is explained by the A-site (Cu<sup>2+</sup>) conduction in CaCu<sub>3</sub>Ru<sub>4-x</sub>Mn<sub>x</sub>O<sub>12</sub>. The thermopower of CaCu<sub>3</sub>Ru<sub>4-x</sub>Mn<sub>x</sub>O<sub>12</sub> was found to be influenced by the substitution, and a sign inversion was observed in the substituted samples at low temperature. The partial substitution of Ru by Mn in CaCu<sub>3</sub>Ru<sub>4</sub>O<sub>12</sub> enables the reduction of the materials cost while maintaining good electrical conductivity for applications as a conducting device component.

**Keywords:** conducting oxide; composite; perovskite; substitution

## 1. Introduction

Perovskites of the general formula AC<sub>3</sub>B<sub>4</sub>O<sub>12</sub> represent a large family of materials and can be considered as a fourfold superstructure of the ABO<sub>3</sub> perovskite in which a cation (A-site) and Jahn-Teller ions (C-site; Cu<sup>2+</sup>, Mn<sup>3+</sup>) are long-range ordered in a double-cubic unit cell. A wide variety of cations can occupy the A-, B- and C-sites, and various partial substitutions are possible on each of these sites [1–6]. Many interesting properties have been found in these compounds, leading to potential applications in various fields. For instance, CaCu<sub>3</sub>Ti<sub>4</sub>O<sub>12</sub> and CaMn<sub>3-x</sub>Cu<sub>x</sub>Mn<sub>4</sub>O<sub>12</sub> show an anomalously high dielectric constant and a giant magneto-resistance, respectively [4,5,7–9]; LaCu<sub>3</sub>Fe<sub>4</sub>O<sub>12</sub> is a negative thermal expansion material [10]; and CaCu<sub>3</sub>Ru<sub>4</sub>O<sub>12</sub> exhibits high metallic electrical conductivity [11,12]. Figure 1 shows the crystal structure of CaCu<sub>3</sub>Ru<sub>4</sub>O<sub>12</sub>. Ca<sup>2+</sup> and Cu<sup>2+</sup> share the A-site of the perovskite. The Ru-ions (Ru<sup>4+</sup>) occupy the B-site at the point (1/4, 1/4, 1/4) of the lattice. The O-ions (O<sup>2-</sup>) are shifted from their regular position at (1/4, 1/4, 0) in simple perovskites as the RuO<sub>6</sub> octahedra are tilted [13].

Recently, many high-temperature operating electrical devices such as gas sensors and solid oxide fuel cells have been actively developed. Their conductive materials are required to be stable at high

temperatures and in various atmospheres [14–20]. Platinum is conventionally used as the conductive materials in such devices, but its high cost has been a serious barrier to their widespread use. Owing to their stability at high temperatures, oxides appear as a potential alternative to platinum, provided they exhibit low resistivity. Among the conducting metal oxides, noble-metal oxides such as  $\text{RuO}_2$  [21],  $\text{IrO}_2$  [21,22], and  $\text{ReO}_2$  [23] exhibit the lowest resistivity. Next comes  $\text{CaCu}_3\text{Ru}_4\text{O}_{12}$ , with a resistivity value at room temperature below  $0.5 \text{ m}\Omega\text{cm}$ , which is one order of magnitude lower than that of La-Sr-Co-Fe-O perovskites (over  $10 \text{ m}\Omega\text{cm}$ ) at room temperature [24]. Therefore,  $\text{CaCu}_3\text{Ru}_4\text{O}_{12}$  is a suitable candidate to replace platinum in devices. However, there are two main challenges with the use of  $\text{CaCu}_3\text{Ru}_4\text{O}_{12}$  in devices. One is its resistance to sintering, but we have found that a possible solution to this issue is to use CuO as a sintering additive [25]. The other is the high cost of Ru. Fortunately, various alternative elements are expected to substitute Ru on the B-site to reduce the material cost of  $\text{CaCu}_3\text{Ru}_4\text{O}_{12}$  while keeping its resistivity low. In addition, the electrical conducting mechanism in  $\text{CaCu}_3\text{Ru}_4\text{O}_{12}$  has been investigated by Kobayashi et al [11], who have shown that not only the Ru-O network, but also  $\text{Cu}^{2+}$  through Kondo coupling [9] between Ru 4d and Cu 3d electrons contributes to the good electrical conduction of the material. This result encourages our scheme to reduce the amount of Ru in  $\text{CaCu}_3\text{Ru}_4\text{O}_{12}$  by substitution while maintaining a high electrical conductivity. In order to use conducting oxides as substitute materials for platinum, their resistivity should be a few  $\text{m}\Omega\text{cm}$  over  $500^\circ\text{C}$  and show a temperature dependence similar to that of metal.

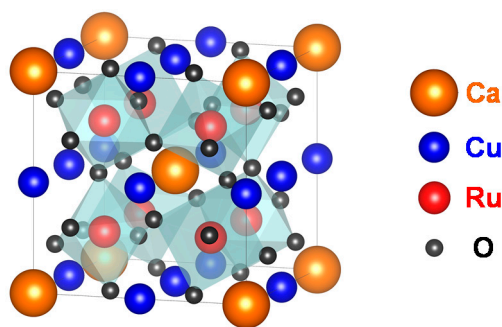


**Figure 1.** Crystal structure of  $\text{CaCu}_3\text{Ru}_4\text{O}_{12}$ . (The figure was drawn using VESTA [26].)

In this study, we focused on Mn as a substitute element for Ru in  $\text{CaCu}_3\text{Ru}_4\text{O}_{12}$  with a fixed amount of sintering additive of 20 vol.% CuO. While the crystal structure and magnetism of  $\text{CaCu}_3\text{Ru}_{4-x}\text{Mn}_x\text{O}_{12}$  have been discussed in a previous report [6], no detailed information on the conducting properties of the material is available. Here, the transport properties of 20 vol.% CuO-mixed  $\text{CaCu}_3\text{Ru}_{4-x}\text{Mn}_x\text{O}_{12}$  with various Mn substitution amounts (in the range 0.00–2.00) were investigated over a wide temperature range (8–900 K).

## 2. Experimental Procedure

$\text{CaCu}_3\text{Ru}_{4-x}\text{Mn}_x\text{O}_{12}$  powders with various Mn substitution amounts ( $x = 0.00, 0.25, 0.50, 0.75, 1.00, 1.25, 1.50, 1.75$  and  $2.00$ ) were prepared by a solid-state reaction method. Stoichiometric mixtures of  $\text{CaCO}_3$ , CuO,  $\text{RuO}_2$ , and  $\text{Mn}_3\text{O}_4$  were pressed into pellets and calcined in air at  $1000^\circ\text{C}$  for 48 h. During calcination, the pellets were surrounded by a mixture of  $\text{CaCO}_3$ , CuO, and  $\text{RuO}_2$  powders to prevent the sublimation of Ru and a consequent composition deviation. In our preliminary experiment, Ru sublimation and formation of second phases such as  $\text{CaRuO}_3$  were confirmed after calcination at  $1000^\circ\text{C}$  without the surroundings. In addition, although the exact solubility limit of Mn at the Ru-site obtained with a synthesis at atmospheric pressure is unknown, it was not possible to synthesize  $\text{CaCu}_3\text{RuMn}_3\text{O}_{12}$  ( $x = 3$ ) with this synthesis method.

$\text{CaCu}_3\text{Ru}_{4-x}\text{Mn}_x\text{O}_{12}$  powders were obtained via the mechanical grinding of the calcined pellets. The  $\text{CaCu}_3\text{Ru}_{4-x}\text{Mn}_x\text{O}_{12}$  powders were then mixed with CuO powder acting as a sintering additive,

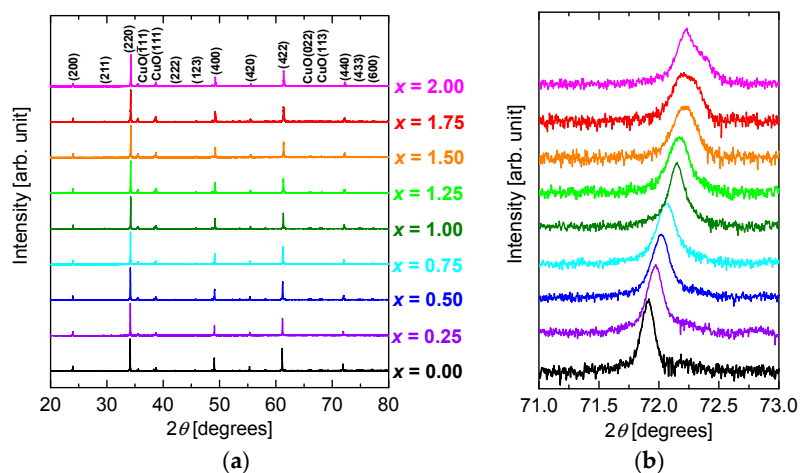
pressed into a pellet, and sintered at 1000 °C for 48 h in air. The obtained samples are hereafter referred to as CuO(20 vol.%)–CaCu<sub>3</sub>Ru<sub>4–x</sub>Mn<sub>x</sub>O<sub>12</sub> bulks. A CuO volume fraction of 20 vol.% was calculated using the molecular weights and lattice constants for each Mn substitution amount. Twenty vol.% of the samples with  $x = 0.00, 0.25, 0.50, 0.75, 1.00, 1.25, 1.50, 1.75$ , and  $2.00$  correspond to 19.6, 19.7, 19.8, 19.9, 20.0, 20.1, 20.1, 20.2, and 20.4 wt%, respectively.

X-ray diffraction (XRD) of the bulk samples was carried out using a standard diffractometer with CuK $\alpha$  radiation, in the  $2\theta$ – $\theta$  scan mode (Rigaku SmartLab, Tokyo, Japan). The morphology of the bulk samples was observed using a field emission scanning electron microscope (FE-SEM; JEOL JSM-6335FM, Tokyo, Japan). The resistivity and thermopower were measured from 7 K to 350 K using a conventional four-probe method and a steady-state technique in vacuum using a cryostat, and from 350 K to 900 K by a four-point probe method in air using an electrical conductivity and Seebeck coefficient measurement system (Ozawa Science RZ2001S, Nagoya, Japan). Since we used different methods and devices for the resistivity measurements below and above 350 K, the value of the resistivity at 350 K obtained with each method differed slightly for each sample. The error is considered to be due to the measurement error of the distance between the voltage terminals in the low-temperature measurements, and the difference between the high-temperature and low-temperature measurement values was less than 10%. Consequently, we normalized the low-temperature data so that the value found at 350 K by the low-temperature method matches that found at 350 K by the high-temperature method. An excellent agreement between the derivative of the two datasets at 350 K was found in all samples.

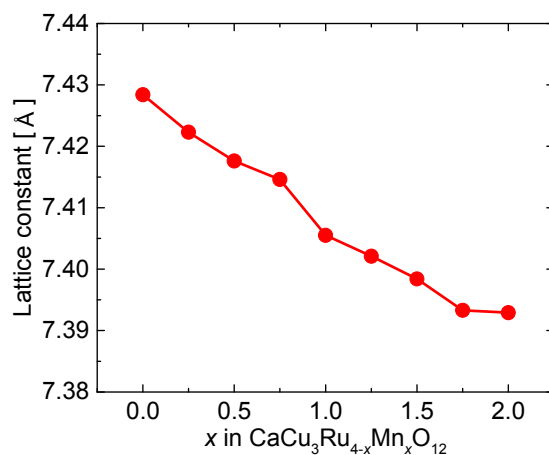
### 3. Results and Discussion

Figure 2a shows the XRD patterns of CuO(20 vol.%)–CaCu<sub>3</sub>Ru<sub>4–x</sub>Mn<sub>x</sub>O<sub>12</sub> bulks for  $x$  varying between 0.00 and 2.00. All the patterns are similar, displaying peaks that can be assigned to CaCu<sub>3</sub>Ru<sub>4</sub>O<sub>12</sub> phase and CuO, respectively. The peaks corresponding to diffraction by the (440) planes of CaCu<sub>3</sub>Ru<sub>4</sub>O<sub>12</sub> phase are enlarged in Figure 2b. The peaks are systematically shifted to higher diffraction angles with increasing  $x$ , indicating that the lattice constant of the sample decreased as  $x$  increased. The lattice constant, which was calculated from the  $2\theta$  angles corresponding to ( $n00$ ) planes, is plotted as a function of  $x$  in Figure 3. The lattice constant systematically decreases from 7.428 Å for CaCu<sub>3</sub>Ru<sub>4</sub>O<sub>12</sub> to 7.393 Å for CaCu<sub>3</sub>Ru<sub>2</sub>Mn<sub>2</sub>O<sub>12</sub> with increasing  $x$ . As a charge transfer from (Ru<sup>4+</sup> + Mn<sup>4+</sup>) to (Ru<sup>5+</sup> + Mn<sup>3+</sup>) has been reported to take place in SrMn<sub>1–y</sub>Ru<sub>y</sub>O<sub>3</sub> [27], we should consider this possibility in CaCu<sub>3</sub>Ru<sub>4–x</sub>Mn<sub>x</sub>O<sub>12</sub> as well. In both cases, given the respective ion size (Ru<sup>4+</sup>: 0.62 Å, Ru<sup>5+</sup>: 0.565 Å, Mn<sup>3+</sup>: 0.645 Å, and Mn<sup>4+</sup>: 0.53 Å), the shift observed in the XRD spectra can be explained by the smaller average size of the ions on the B-site of the substituted material (either Mn<sup>4+</sup> and Ru<sup>4+</sup>, or Mn<sup>3+</sup> and Ru<sup>5+</sup>) with respect to that of Ru<sup>4+</sup>, even if the size reduction effect would be larger without the charge transfer. By contrast, the influence of such a charge transfer on the electrical transport and resistivity would be dramatically large. In light of our resistivity measurements discussed below, which show no such dramatic change upon substitution, we can infer that the valence of Ru did not change.

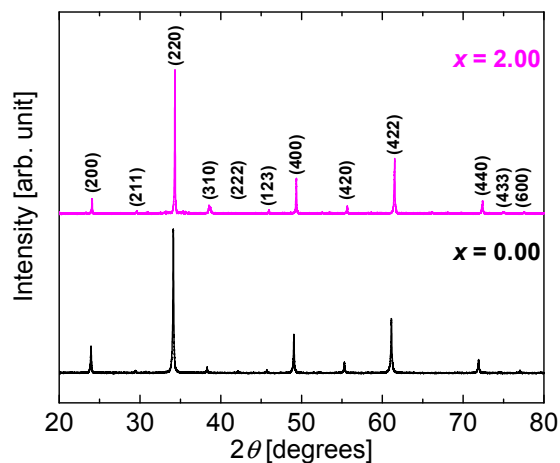
Figure 4 shows the XRD patterns of as-synthesized CaCu<sub>3</sub>Ru<sub>4</sub>O<sub>12</sub> and CaCu<sub>3</sub>Ru<sub>2</sub>Mn<sub>2</sub>O<sub>12</sub> powders. The patterns of both are almost the same, and there are no peaks corresponding to the raw materials or some second phases. We accurately weighed the raw materials according to the stoichiometry of CaCu<sub>3</sub>Ru<sub>2</sub>Mn<sub>2</sub>O<sub>12</sub>. Therefore, if we assume that Mn could substitute Cu, yielding CaCu<sub>3–y</sub>Mn<sub>y</sub>Ru<sub>4–x</sub>Mn<sub>x</sub>O<sub>12</sub>, then the composition ratio of the raw materials would not match that of the formed compound, and some peaks corresponding to the raw materials and/or second phases would be observed in the XRD patterns. From this result, we consider that a very small quantity of Mn may have substituted Cu. In Figure 2b, the peaks corresponding to the (440) plane of CaCu<sub>3</sub>Ru<sub>2.25</sub>Mn<sub>1.75</sub>O<sub>12</sub> and CaCu<sub>3</sub>Ru<sub>2</sub>Mn<sub>2</sub>O<sub>12</sub> are broader than those of the other samples. This broadening may due to a phase separation between the phases with and without Cu–Mn substitution in the samples with high Mn substitution.



**Figure 2.** XRD ( $\text{CuK}\alpha$ ) patterns of the  $\text{CuO}(20 \text{ vol.}\%)\text{--CaCu}_3\text{Ru}_{4-x}\text{Mn}_x\text{O}_{12}$  bulks. (a) Patterns between  $20^\circ$  and  $80^\circ$ . The peak labels without ‘CuO’ correspond to the  $\text{CaCu}_3\text{Ru}_4\text{O}_{12}$  phase. (b) Enlarged patterns ( $71^\circ\text{--}73^\circ$ ) for the peaks corresponding to diffraction by the (440) planes of the  $\text{CaCu}_3\text{Ru}_4\text{O}_{12}$  phase.

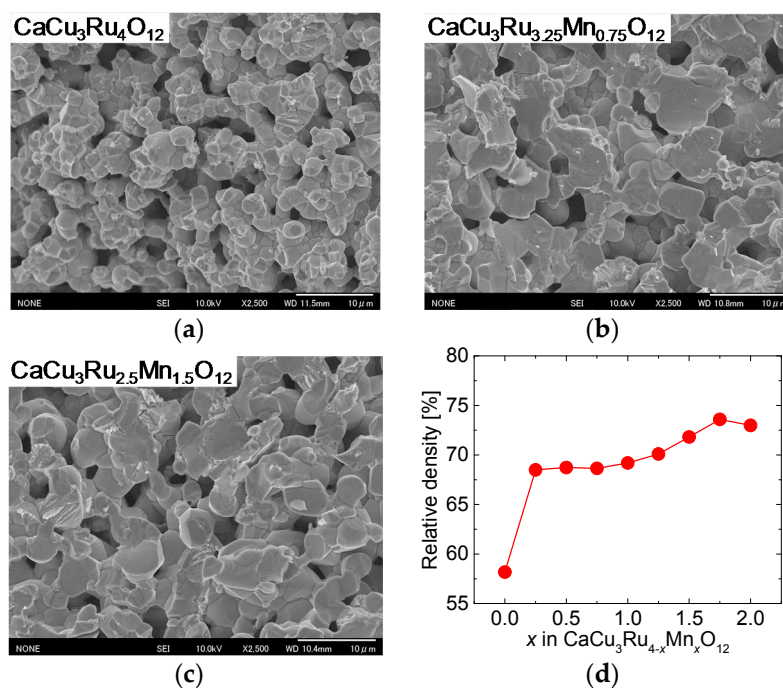


**Figure 3.** Lattice constant of  $\text{CaCu}_3\text{Ru}_{4-x}\text{Mn}_x\text{O}_{12}$  in the  $\text{CuO}(20 \text{ vol.}\%)\text{--CaCu}_3\text{Ru}_{4-x}\text{Mn}_x\text{O}_{12}$  bulks plotted as a function of Mn substitution amount  $x$ .



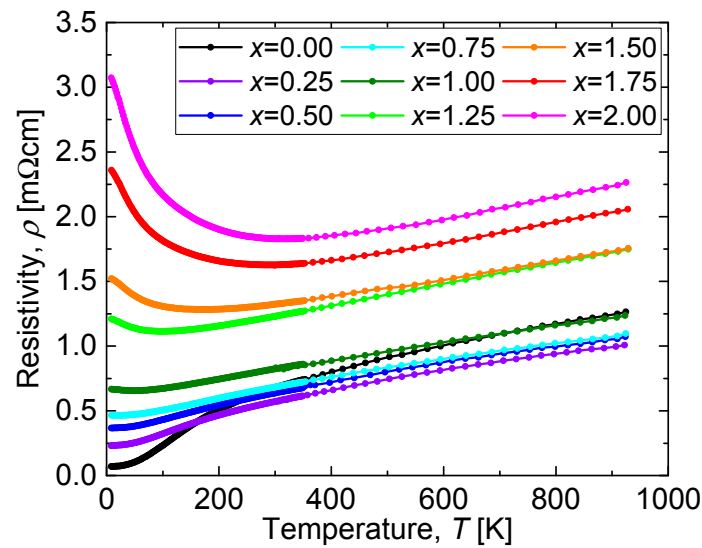
**Figure 4.** XRD ( $\text{CuK}\alpha$ ) patterns of the as-synthesized  $\text{CaCu}_3\text{Ru}_4\text{O}_{12}$  and  $\text{CaCu}_3\text{Ru}_2\text{Mn}_2\text{O}_{12}$  powders.

Figure 5a through c show FE-SEM images of the surface of the samples with  $x = 0.00$ , 0.75, and 1.50, respectively. In all samples, the grains fused together, and there are a lot of voids. The diameter of the grain was about 3 and 5  $\mu\text{m}$  without and with Mn substitution, respectively. The grain size in the samples with Mn substitution was observed to be almost the same for all values of  $x \neq 0.00$ . As it depends on the grain size, the thickness of the necks between the grains was larger in the substituted samples than in the unsubstituted sample. Figure 5d shows the relative density of  $\text{CuO}(20 \text{ vol.}\%)\text{-CaCu}_3\text{Ru}_{4-x}\text{Mn}_x\text{O}_{12}$  bulks as a function of  $x$ . The relative density displayed a dramatic increase between  $x = 0.00$  (unsubstituted sample) and  $x = 0.25$ , and then slightly increased with increasing  $x$ . The results shown in Figure 5 suggest that Mn substitution increased the defect density, which promoted volume diffusion, and, in turn, grain growth and densification of the  $\text{CaCu}_3\text{Ru}_{4-x}\text{Mn}_x\text{O}_{12}$  phase.



**Figure 5.** FE-SEM images of the surface of the  $\text{CuO}(20 \text{ vol.}\%)\text{-CaCu}_3\text{Ru}_{4-x}\text{Mn}_x\text{O}_{12}$  bulks with  $x = 0.00$  (a), 0.75 (b), and 1.50 (c). (d) Relative density of the samples as a function of  $x$ .

The temperature dependence of the resistivity ( $\rho$ - $T$  curve) of the  $\text{CuO}(20 \text{ vol.}\%)\text{-CaCu}_3\text{Ru}_{4-x}\text{Mn}_x\text{O}_{12}$  bulks is shown in Figure 6. The resistivity systematically increased with increasing  $x$  except for the sample with  $x = 0.00$ , which is attributed to its lower relative density with respect to the other (Mn-substituted) samples. A  $\text{CaCu}_3\text{Ru}_4\text{O}_{12}$  bulk sample prepared with a similar relative density to that of the Mn-substituted samples would be expected to have a lower resistivity than that of the sample with  $x = 0.25$ . It is noteworthy that the resistivity value was always as low as a few  $\text{m}\Omega\text{cm}$ , even in the sample with  $x = 2.00$ , which contains as many Mn as Ru ions. In the case of other perovskite materials with Ru-Mn substitution such as  $\text{CaRu}_{1-x}\text{Mn}_x\text{O}_3$  and  $\text{SrRu}_{1-x}\text{Mn}_x\text{O}_3$ , the substitution of half of the Ru-sites with Mn causes a drastic increase in the resistivity or band gap [28,29]. In particular, the resistivity increases at 300 K from 2  $\text{m}\Omega\text{cm}$  for  $\text{SrRuO}_3$  to 20  $\text{m}\Omega\text{cm}$  for  $\text{SrRu}_{0.5}\text{Mn}_{0.5}\text{O}_3$ . In these materials, Ru 4d electrons are responsible for electrical conduction, while Mn substitution reduces the overlaps between the electron clouds. However, as mentioned in the introduction, in the case of  $\text{CaCu}_3\text{Ru}_4\text{O}_{12}$ , electrons from the A-site ( $\text{Cu}^{2+}$ ) are also responsible for electrical conduction [11], which explains the low resistivity of  $\text{CaCu}_3\text{Ru}_2\text{Mn}_2\text{O}_{12}$ .



**Figure 6.** Temperature dependence of the resistivity of CuO(20 vol.%)–CaCu<sub>3</sub>Ru<sub>4–x</sub>Mn<sub>x</sub>O<sub>12</sub> bulks.

While the resistivity systematically increased with increasing  $x$ , it showed the same temperature dependence at high temperatures for all values of  $x$ . The reason for this is that phonon scattering following Matthiessen's rule is the dominant parameter that influences the electrical resistivity at temperatures above 300 K. On the other hand, the temperature dependence of the resistivity at low temperatures differed according to the value of  $x$ . The residual resistivity  $\rho(T = 0)$  increased with increasing  $x$  below  $x = 1.00$ . Above  $x = 1.25$ , the resistivity increased with cooling, which corresponds to a semiconducting behavior.

Let us analyze the semiconducting behavior at low temperatures of Mn-substituted samples using two kinds of transport mechanism, the activated conduction and the hopping conduction, which are representative conduction mechanisms for semiconducting electrical transport. Parts of the  $\rho$ - $T$  curves corresponding to a transport mechanism dominated by activated conduction can be fitted by the following equation:

$$\rho = \rho_0 \exp(E_g/k_B T), \quad (1)$$

where  $k_B$ ,  $T$ , and  $E_g$  are the Boltzmann constant, absolute temperature, and activation energy, respectively. In that way, the activation energy, i.e., the transport gap  $E_g$ , can be determined. Figure 7a shows  $\ln(\rho/\text{m}\Omega\text{cm})$  plotted against  $T^{-1}$  for CaCu<sub>3</sub>Ru<sub>2</sub>Mn<sub>2</sub>O<sub>12</sub>. The fitting curve corresponding to Equation (1) is shown as a broken line. The plot was well fitted by Equation (1) between  $T^{-1} = 5.563 \times 10^{-3}$  (i.e.,  $T = 179.76$  K) and  $4.204 \times 10^{-3}$  (i.e.,  $T = 237.86$  K), in good agreement with the minimal value of the resistivity showed in Figure 6. From the fitting curve, the activation energy, expressed as a temperature, was determined as  $E_g/k_B = 30.28$  K. This temperature is much lower than the temperature at which semiconducting behavior begins, indicating that activated conduction is not employed in CaCu<sub>3</sub>Ru<sub>2</sub>Mn<sub>2</sub>O<sub>12</sub> at low temperatures; hopping conduction is the conduction mechanism at work.

Variable range hopping (VRH) conduction is one type of hopping conduction that gives rise to a temperature dependence of the resistivity of the form [30]:

$$\rho = \rho_0 \exp(U/T^{1/4}). \quad (2)$$

Figure 7b shows  $\ln(\rho/\text{m}\Omega\text{cm})$  plotted against  $T^{-1/4}$  for CaCu<sub>3</sub>Ru<sub>2</sub>Mn<sub>2</sub>O<sub>12</sub>. The broken line is the fitting curve obtained with Equation (2). The fitting line fits to the plot for  $T^{-1/4}$  between 0.3612 (i.e.,  $T = 58.76$  K) and 0.2609 (i.e.,  $T = 215.89$  K). This temperature range roughly corresponds to the temperature region where CaCu<sub>3</sub>Ru<sub>2</sub>Mn<sub>2</sub>O<sub>12</sub> showed semiconducting behavior according to

the  $\rho$ - $T$  curve shown in Figure 6. Accordingly, it can be concluded that the conducting mechanism in  $\text{CaCu}_3\text{Ru}_2\text{Mn}_2\text{O}_{12}$  at low temperatures is VRH conduction. Hopping conduction occurs due to the discontinuity of Ru conduction caused by Mn substitution, which explains the expansion of the temperature range of the semiconducting behavior to higher temperatures with increasing  $x$ , as shown in Figure 6.

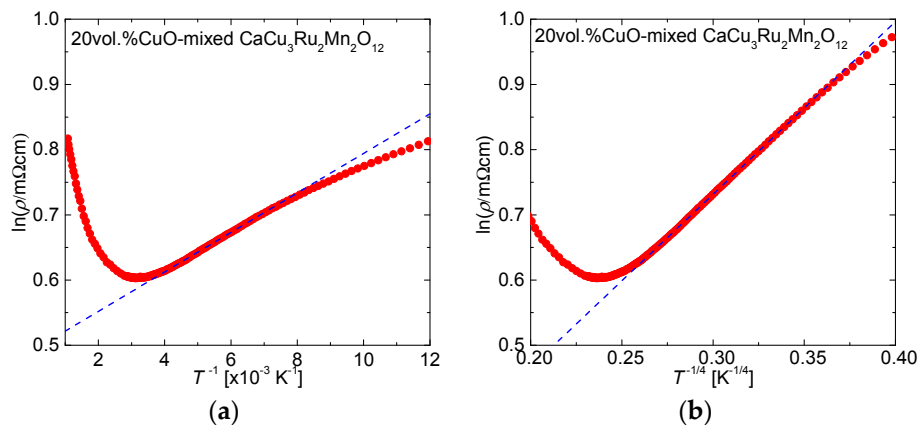


**Figure 7.** Temperature dependence of the resistivity of CuO(20 vol.%)– $\text{CaCu}_3\text{Ru}_2\text{Mn}_2\text{O}_{12}$  (a) Plot of  $\ln(\rho/\text{m}\Omega\text{cm})$  against  $T^{-1}$  (b) Plot of  $\ln(\rho/\text{m}\Omega\text{cm})$  against  $T^{-1/4}$ . The broken lines correspond to active conduction (a) and variable range hopping (b) as given by Equations (1) and (2), respectively.

From these results, it appears that two electrical conduction mechanisms underlie the electrical conduction in  $\text{CaCu}_3\text{Ru}_{4-x}\text{Mn}_x\text{O}_{12}$ , as schematically shown in Figure 8. As reported in previous reports,  $\text{CaCu}_3\text{Ru}_4\text{O}_{12}$  ( $x = 0$ ) exhibits two kinds of electrical current paths (Figure 8a). The first one relies on the Ru–O network ( $I_{\text{Ru}}$ ), while the second relies on  $\text{Cu}^{2+}$  ( $I_{\text{Cu}}$ ). In the case of  $x \neq 0$  (Figure 8b), the substitution of part of the Ru sites with Mn disrupts the conducting Ru–O network, and conduction electrons hop on to the Mn sites along their path ( $I_{\text{Ru+Mn}}$ ). Hopping slows down the electrons, therefore  $I_{\text{Ru+Mn}}$  is smaller than  $I_{\text{Ru}}$ . However, the decrease in the total conduction current intensity is small as  $I_{\text{Cu}}$  is not affected by the presence of Mn.

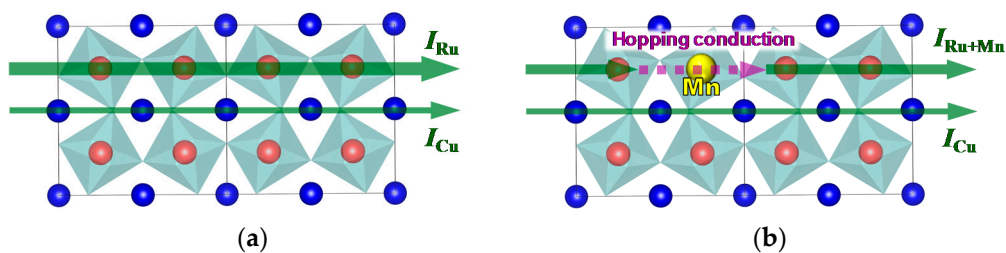


**Figure 8.** Schematic of  $\text{CaCu}_3\text{Ru}_{4-x}\text{Mn}_x\text{O}_{12}$  in real space showing the different paths for electrical conduction when (a)  $x = 0$ , and (b)  $x \neq 0$ . For simplicity, Ca and O ions are omitted. ( $\text{CaCu}_3\text{Ru}_{4-x}\text{Mn}_x\text{O}_{12}$  lattices were drawn using VESTA [26].)

Figure 9 shows the temperature dependence of the thermopower  $S$  ( $S$ - $T$  curve) of the CuO(20 vol.%)– $\text{CaCu}_3\text{Ru}_{4-x}\text{Mn}_x\text{O}_{12}$  bulks. Similarly to the  $\rho$ - $T$  curves, the  $S$ - $T$  curves exhibit a systematic variation with  $x$ . The thermopower of all samples decreased with cooling, and the thermopower of the Mn-substituted samples was negative at low temperatures, while that of  $\text{CaCu}_3\text{Ru}_4\text{O}_{12}$  was positive. A similar effect was observed for  $\text{Ca}_{0.5}\text{Sr}_{0.5}\text{RuO}_3$  and  $\text{Ca}_{0.5}\text{Sr}_{0.5}\text{Ru}_{0.5}\text{Mn}_{0.5}\text{O}_3$ , whose thermopower between 10 and 280 K is respectively positive and negative between 10 and 280 K, explained by the fact that the Ru–Mn substitution changes the majority carrier from holes to electrons [28]. The temperature range in which the thermopower of the CuO(20 vol.%)– $\text{CaCu}_3\text{Ru}_{4-x}\text{Mn}_x\text{O}_{12}$  bulks

is negative increased with increasing  $x$ , indicating that a gradual change of majority carrier took place in the CuO(20 vol.%)–CaCu<sub>3</sub>Ru<sub>4–x</sub>Mn<sub>x</sub>O<sub>12</sub> bulks with increasing  $x$ . This Mn substitution effect is considered to be weaker in CaCu<sub>3</sub>Ru<sub>4–x</sub>Mn<sub>x</sub>O<sub>12</sub> than in Ca<sub>0.5</sub>Sr<sub>0.5</sub>Ru<sub>1–x</sub>Mn<sub>x</sub>O<sub>3</sub> because of the A-site-based electrical conduction, which, as already mentioned, is not affected by B-site substitution.

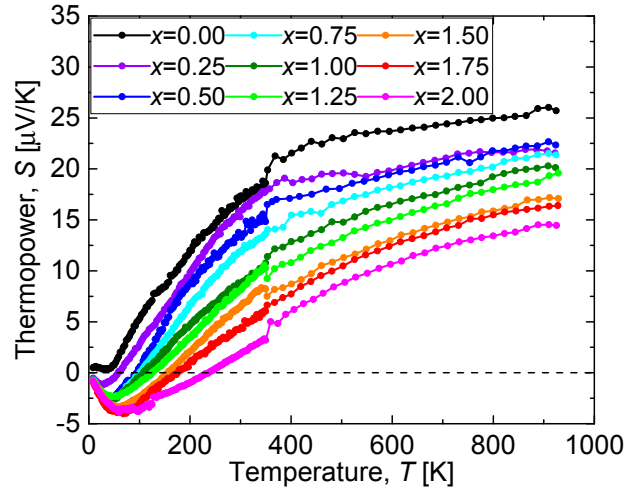


**Figure 9.** Temperature dependence of the thermopower of CuO(20 vol.%)–CaCu<sub>3</sub>Ru<sub>4–x</sub>Mn<sub>x</sub>O<sub>12</sub> bulks.

It has been reported that the temperature dependence of the thermopower in the case of VRH conduction is of the form:  $S = T^{1/2}$  [31]. Figure 10 shows the thermopower  $S$  of CaCu<sub>3</sub>Ru<sub>2</sub>Mn<sub>2</sub>O<sub>12</sub> plotted against  $T^{1/2}$ . Although VRH conduction was observed below 215.89 K in the resistivity curve (215.89 K corresponds to  $T^{1/2} = 14.7 \text{ K}^{1/2}$ , shown as a black dash line in Figure 10), the fitting line in Figure 10 (shown as a red solid line) corresponding to  $|S| = aT^{1/2} + b$  indicates VRH conduction below  $T^{1/2} = 7 \text{ K}^{1/2}$  ( $T = 49 \text{ K}$ , shown as a blue dot line). This discrepancy can be explained by the fact that the fitting equation for  $S$  has been derived from a model of an amorphous semiconductor with a single type of carrier, while both electrons and holes are electrical carriers in CaCu<sub>3</sub>Ru<sub>4–x</sub>Mn<sub>x</sub>O<sub>12</sub>. As  $S$  is strongly affected by the type of carrier, the red fitting line in Figure 10 fitted the  $S(T^{1/2})$  curve only at very low temperatures, because holes lose mobility at these temperatures and electrons can be considered as the only charge carriers.

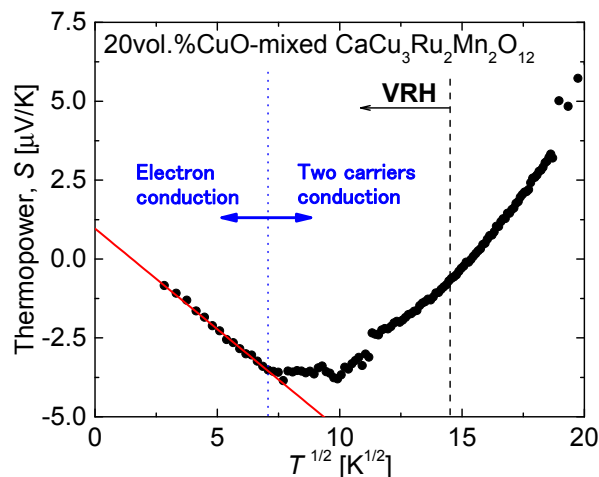


**Figure 10.** Thermopower of CuO(20 vol.%)–CaCu<sub>3</sub>Ru<sub>2</sub>Mn<sub>2</sub>O<sub>12</sub> bulks plotted against  $T^{1/2}$ . The red solid line corresponds to the fitting equation  $|S| = aT^{1/2} + b$ .

#### 4. Conclusions

We prepared CuO(20 vol.%)–CaCu<sub>3</sub>Ru<sub>4–x</sub>Mn<sub>x</sub>O<sub>12</sub> bulks with various substitution amounts  $x$ , and investigated the influence of  $x$  on the electrical resistivity. Only the CuO and CaCu<sub>3</sub>Ru<sub>4–x</sub>Mn<sub>x</sub>O<sub>12</sub> phases were detected by XRD in all samples, and a peak shift due to the substitution was confirmed. SEM observations and a calculation of the relative density showed an enhancement of the grain growth and sintering with increasing substitution. The resistivity increased with increasing  $x$ , but all samples maintained good conductivity with resistivity as low as a few mΩcm, even in the sample with  $x = 2.00$ . This phenomenon is explained by the existence of A-site (Cu<sup>2+</sup>) conduction in CaCu<sub>3</sub>Ru<sub>4–x</sub>Mn<sub>x</sub>O<sub>12</sub>. The temperature dependence of the resistivity of CuO(20 vol.%)–CaCu<sub>3</sub>Ru<sub>4–x</sub>Mn<sub>x</sub>O<sub>12</sub> bulks indicated a semiconducting behavior at low temperatures. The conduction mechanism at low temperatures was identified as variable range hopping conduction, where hopping occurs because the Ru conduction path is disrupted by the presence of Mn on Ru sites. The thermopower was found to be affected by the substitution as well. In particular, a sign inversion of the thermopower was observed in the substituted samples at low temperatures. This study therefore demonstrates that the partial substitution of Ru by Mn in CaCu<sub>3</sub>Ru<sub>4</sub>O<sub>12</sub> is an excellent strategy to reduce the material cost while maintaining good conductivity.

**Acknowledgments:** The authors thank Takara Hiroi (AIST, Japan) for her experimental assistance.

**Author Contributions:** A.T., I.T. and W.S. conceived and designed the experiments; A.T. performed the experiments; A.T., I.T. and W.S. analyzed the data; M.M., Y.K. and N.M. helped experiments and discussed about results; A.T. wrote the paper.

**Conflicts of Interest:** The authors declare no conflict of interest.

#### References

- Marezio, M.; Dernier, P.D.; Chenavas, J.; Joubert, J.C. High pressure synthesis and crystal structure of NaMn<sub>7</sub>O<sub>12</sub>. *J. Solid State Chem.* **1973**, *6*, 16–20. [[CrossRef](#)]
- Andres, K.; Graebner, J.E.; Ott, H.R. 4f-Virtual-Bound-State Formation in CeAl<sub>3</sub> at Low Temperatures. *Phys. Rev. Lett.* **1975**, *35*, 1779–1782. [[CrossRef](#)]
- Bochu, B.; Deschizeaux, M.N.; Joubert, J.C.; Collomb, A.; Chenavas, J.; Marezio, M. Synthèse et caractérisation d'une série de titanates pérovskites isotypes de [CaCu<sub>3</sub>](Mn<sub>4</sub>)O<sub>12</sub>. *J. Solid State Chem.* **1979**, *29*, 291–298. [[CrossRef](#)]
- Subramanian, M.A.; Li, D.; Duan, N.; Reisner, B.A.; Sleight, A.W. High Dielectric Constant in ACu<sub>3</sub>Ti<sub>4</sub>O<sub>12</sub> and ACu<sub>3</sub>Ti<sub>3</sub>FeO<sub>12</sub> Phases. *J. Solid State Chem.* **2000**, *151*, 323–325. [[CrossRef](#)]
- Subramanian, M.A.; Sleight, A.W. ACu<sub>3</sub>Ti<sub>4</sub>O<sub>12</sub> and ACu<sub>3</sub>Ru<sub>4</sub>O<sub>12</sub> perovskites: High dielectric constants and valence degeneracy. *Solid State Sci.* **2002**, *4*, 347–351. [[CrossRef](#)]
- Calle, C.; Sánchez-Benítez, J.; Barbanson, F.; Nemes, N.; Fernández-Díaz, M.T.; Alonso, J.A. Transition from Pauli-paramagnetism to ferromagnetism in CaCu<sub>3</sub>(Ru<sub>4–x</sub>Mn<sub>x</sub>)O<sub>12</sub> (0 ≤  $x$  ≤ 3) perovskites. *J. Appl. Phys.* **2011**, *109*, 123914. [[CrossRef](#)]
- Ramirez, A.P.; Subramanian, M.A.; Gardel, M.; Blumberg, G.; Li, D.; Vogt, T.; Shapiro, S.M. Giant dielectric constant response in a copper-titanate. *Solid State Commun.* **2000**, *115*, 217–220. [[CrossRef](#)]
- Homes, C.C.; Vogt, T.; Shapiro, S.M.; Wakimoto, S.; Ramirez, A.P. Optical Response of High-Dielectric-Constant Perovskite-Related Oxide. *Science* **2001**, *293*, 673–676. [[CrossRef](#)] [[PubMed](#)]
- Kondo, S.; Johnston, D.C.; Swenson, C.A.; Borsa, F.; Mahajan, A.V.; Miller, L.L.; Gu, T.; Goldman, A.I.; Maple, M.B.; Gajewski, D.A.; et al. LiV<sub>2</sub>O<sub>4</sub>: A Heavy Fermion Transition Metal Oxide. *Phys. Rev. Lett.* **1997**, *78*, 3729–3732. [[CrossRef](#)]
- Long, Y.W.; Hayashi, N.; Saito, T.; Azuma, M.; Muranaka, S.; Shimakawa, Y. Temperature-induced A-B intersite charge transfer in an A-site-ordered LaCu<sub>3</sub>Fe<sub>4</sub>O<sub>12</sub> perovskite. *Nature* **2009**, *485*, 60–63. [[CrossRef](#)] [[PubMed](#)]
- Kobayashi, W.; Terasaki, I.; Takeya, J.; Tsukada, I.; Ando, Y. A Novel Heavy-Fermion State in CaCu<sub>3</sub>Ru<sub>4</sub>O<sub>12</sub>. *J. Phys. Soc. Jpn.* **2004**, *73*, 2373–2376. [[CrossRef](#)]

12. Hébert, S.; Daou, R.; Maignan, A. Thermopower in the quadruple perovskite ruthenates. *Phys. Rev. B* **2015**, *91*, 045106. [CrossRef]
13. Ebbinghaus, S.G.; Weidenkaff, A.; Cava, R.J. Structural Investigations of  $ACu_3Ru_4O_{12}$  ( $A = Na, Ca, Sr, La, Nd$ )-Comparison between XRD-Rietveld and EXAFS Results. *J. Solid State Chem.* **2002**, *167*, 126–136. [CrossRef]
14. Fleischer, M.; Meixner, H. Fast gas sensors based on metal oxides which are stable at high temperatures. *Sens. Actuators B Chem.* **1997**, *43*, 1–10. [CrossRef]
15. Esch, H.; Huyberechts, G.; Mertens, R.; Maes, G.; Manca, J.; Ceuninck, W.; Schepper, L. The stability of Pt heater and temperature sensing elements for silicon integrated tin oxide gas sensors. *Sens. Actuators B Chem.* **2000**, *65*, 190–192. [CrossRef]
16. Izu, N.; Shin, W.; Murayama, N. Fast response of resistive-type oxygen gas sensors based on nano-sized ceria powder. *Sens. Actuators B Chem.* **2003**, *93*, 449–453. [CrossRef]
17. Korotcenkov, G.; Cho, B.K. Engineering approaches to improvement of conductometric gas sensor parameters. Part 2: Decrease of dissipated (consumable) power and improvement stability and reliability. *Sens. Actuators B Chem.* **2014**, *198*, 316–341. [CrossRef]
18. Matsuzaki, Y.; Yasuda, I. Electrochemical properties of a SOFC cathode in contact with a chromium-containing alloy separator. *Solid State Ion.* **2000**, *132*, 271–278. [CrossRef]
19. Suzuki, T.; Awano, M.; Jasinski, P.; Petrovsky, V.; Anderson, H.U. Composite (La, Sr)MnO<sub>3</sub>-YSZ cathode for SOFC. *Solid State Ion.* **2006**, *177*, 2071–2074. [CrossRef]
20. Sumi, H.; Yamaguchi, T.; Hamamoto, K.; Suzuki, T.; Fujishiro, Y. High performance of La<sub>0.6</sub>Sr<sub>0.4</sub>Co<sub>0.2</sub>Fe<sub>0.8</sub>O<sub>3</sub>-Ce<sub>0.9</sub>Gd<sub>0.1</sub>O<sub>1.95</sub> nanoparticulate cathode for intermediate temperature microtubular solid oxide fuel cells. *J. Power Sources* **2013**, *226*, 354–358. [CrossRef]
21. Jia, Q.X.; Wu, X.D.; Foltyn, S.R.; Findikoglu, A.T.; Tiwari, P.; Zheng, J.P.; Jow, T.R. Heteroepitaxial growth of highly conductive metal oxide RuO<sub>2</sub> thin films by pulsed laser deposition. *Appl. Phys. Lett.* **1995**, *67*, 1677–1679. [CrossRef]
22. Ryden, W.; Lawson, A.; Sartain, C. Electrical Transport Properties of IrO<sub>2</sub> and RuO<sub>2</sub>. *Phys. Lett. B* **1970**, *1*, 1494–1500.
23. Pearsall, T.P.; Lee, C.A. Electronic transport in ReO<sub>3</sub>: dc conductivity and Hall effect. *Phys. Rev. B* **1974**, *10*, 2190. [CrossRef]
24. Ullmann, H.; Trofimenko, N.; Tietz, F.; Stöver, D.; Ahmad-Khanlou, A. Correlation between thermal expansion and oxide ion transport in mixed conducting perovskite-type oxides for SOFC cathodes. *Solid State Ion.* **2000**, *138*, 79–90. [CrossRef]
25. Tsuruta, A.; Mikami, M.; Kinemuchi, Y.; Terasaki, I.; Murayama, N.; Shin, W. High electrical conductivity of composite ceramics consisting of insulating oxide and ordered perovskite conducting oxide. *Phys. Status Solidi A* **2017**, in press.
26. VESTA. Available online: <http://jp-minerals.org/vesta/en/> (accessed on 1 April 2017).
27. Kolesnik, S.; Dabrowski, B.; Chmaissem, O. Structural and physical properties of SrMn<sub>1-x</sub>Ru<sub>x</sub>O<sub>3</sub> perovskites. *Phys. Rev. B* **2008**, *78*, 214425. [CrossRef]
28. Ohnishi, T.; Naito, M.; Mizusaki, S.; Nagata, Y.; Noro, Y. Transport and Thermoelectric Properties of the Ca<sub>1-x</sub>Sr<sub>x</sub>Ru<sub>1-y</sub>Mn<sub>y</sub>O<sub>3</sub> System. *J. Electron. Mater.* **2011**, *40*, 915–919. [CrossRef]
29. Wang, L.; Hua, L.; Chen, L. F. First-principles investigation of the structural, magnetic and electronic properties of perovskite SrRu<sub>1-x</sub>Mn<sub>x</sub>O<sub>3</sub>. *J. Phys. Condens. Matter* **2009**, *21*. [CrossRef] [PubMed]
30. Quitmann, C.; Andrich, D.; Jarchow, C.; Fleuster, M.; Beschoten, B.; Güntherodt, G.; Moshchalkov, V.V.; Mante, G.; Manzke, R. Scaling behavior at the insulator-metal transition in Bi<sub>2</sub>Sr<sub>2</sub>(Ca<sub>z</sub>R<sub>1-z</sub>)Cu<sub>2</sub>O<sub>8+y</sub> where R is a rare-earth element. *Phys. Rev. B* **1992**, *46*, 11813. [CrossRef]
31. Overhof, H. Thermopower Calculation for Variable Range Hopping-Application to  $\alpha$ -Si. *Phys. Stat. Sol. B* **1975**, *67*, 709. [CrossRef]

